Lab on a Chip RSCPublishing

LAB ON A CHIP

ELECTRONIC SUPPLEMENTARY INFORMATION

TITLE: Functional microengineered model of the human splenon-on-a-chip.

AUTHORS: L.G. Rigat-Brugarolas, A. Elizalde-Torrent, M. Bernabeu, M. De Niz, L. Martin-Jaular, C. Fernandez-Becerra, A. Homs-Corbera, J. Samitier and H.A. del Portillo.

LAB ON A CHIP: ELECTRONIC SUPPLEMENTARY INFORMATION

Figure S1. Electric circuit analogy used to design the microfluidic device.

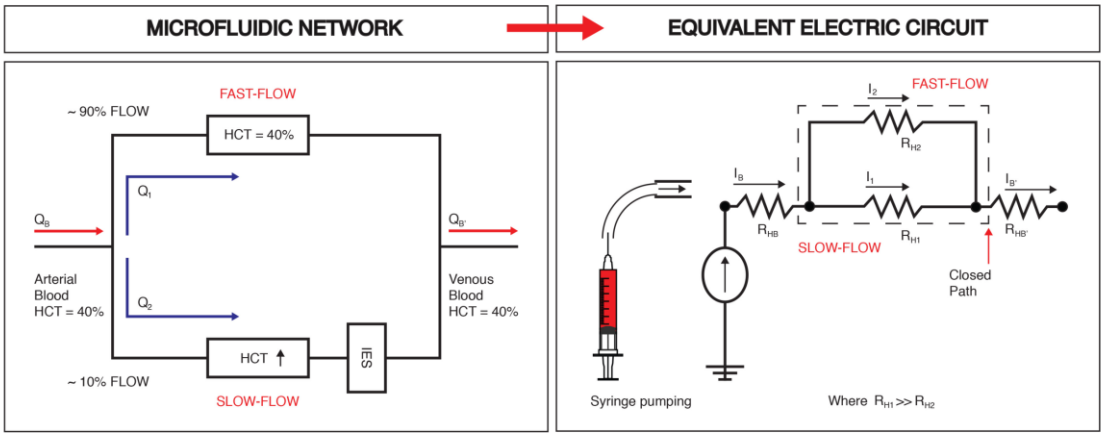

Figure S1. Electric circuit analogy used to design the microfluidic device. Left panel. Diagram shows how the volume flow of arterial blood (Q_B) is divided into two different volume flows, depending on whether it goes through the closed-fast microcirculation (Q_1), where the hematocrit remains at around 40%, or it goes through the open-slow microcirculation (Q_2), where the hematocrit increases and then through IES before encountering each other in the volume flow of the venous bloss ($Q_{B'}$). **Right panel**. The equivalent electric circuit. Depending on which branch of the circuit, the resistance (R) and the current intensity (I) are different. The resistance in the open-slow microcirculation equivalent branch (R_{H1}) is much higher than the resistance in the closed-fast microcirculation equivalent branch (R_{H2}). Q: volume flow; HCT: hematocrit; I: current intensity; R: resistance.

Figure S2. Comsol simulations of the microfluidic device to obtain a correct architecture

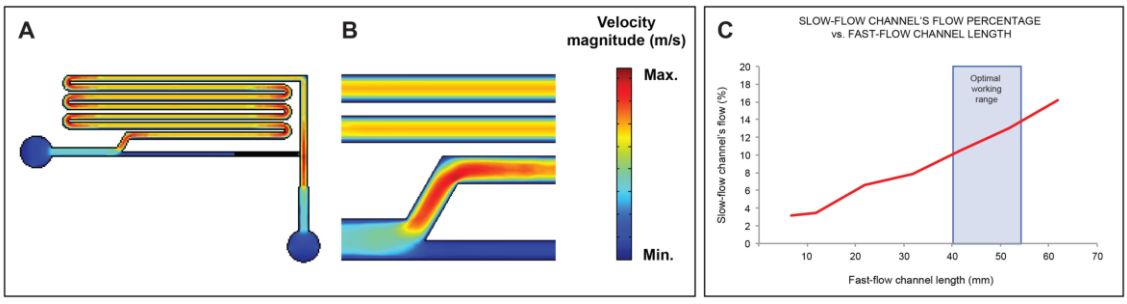

Figure S2. Comsol simulations of the microfluidic device to obtain a correct architecture. Left panel. Diagrams show Comsol Multyphysics simulations showing **(A)** the velocity magnitude in the entire microfluidic device and **(B)** flow division at the bifurcation point (fast-flow channel vs. slow-flow channel). This flow division is independent of the inlet flow rate so depends entirely on the architecture of the device; therefore the calculation of the hydraulic resistance in both channels represents a crucial point for achieving the correct flow division. **Right panel**. Graph representing the slow-flow channel's flow percentage, which is dependent on the fast-flow channel length. The study is addressed within the architecture and dimensions of the slow-flow channel; therefore, diverse fast-flow channel lengths were analyzed.

Figure S3. Experimetal system operation.

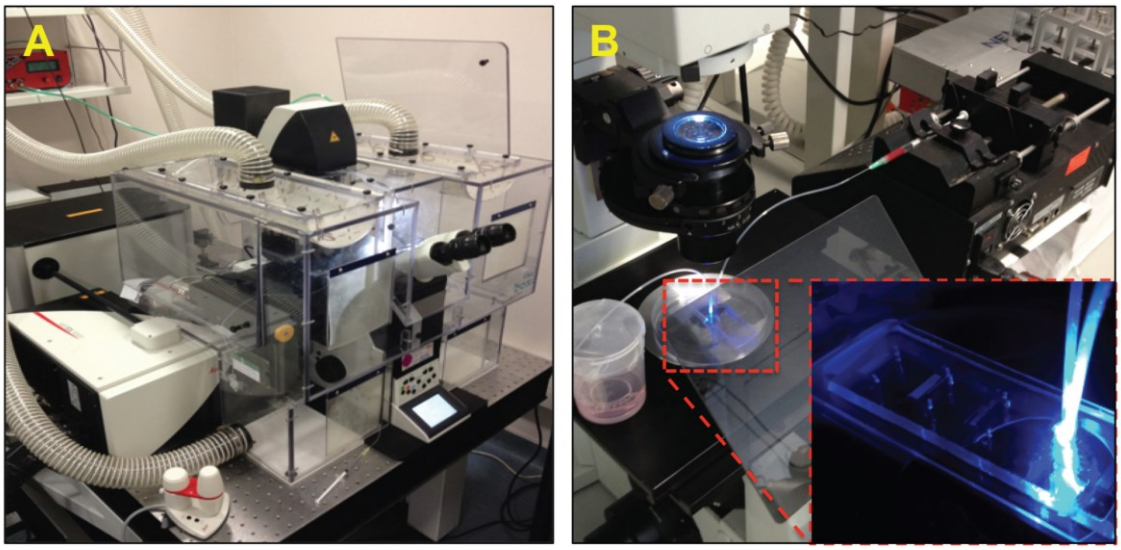

Figure S3. Experimental system operation. (A) Laser scanning confocal microscope TCS-SP5 (Leica Microsystems) where *in vivo* imaging of the mouse spleen was obtained to determine the *in vivo* physiological blood flow rate. **(B)** Images for microfluidic analyses were taken with an inverted optical microscope (Olympus IX71) with an integrated CCD Hamamatsu camera. The experimental setup consists of a 1ml syringe connected through a needle with PTFE tubing to the microfluidic device. The syringe is actuated with a KDS 200 series pump at a constant flow. Tubes were inserted into the access holes which were slightly smaller than the outer diameter of the tubing to form a pressure seal.

Figure S4. Microfluidic device validation.

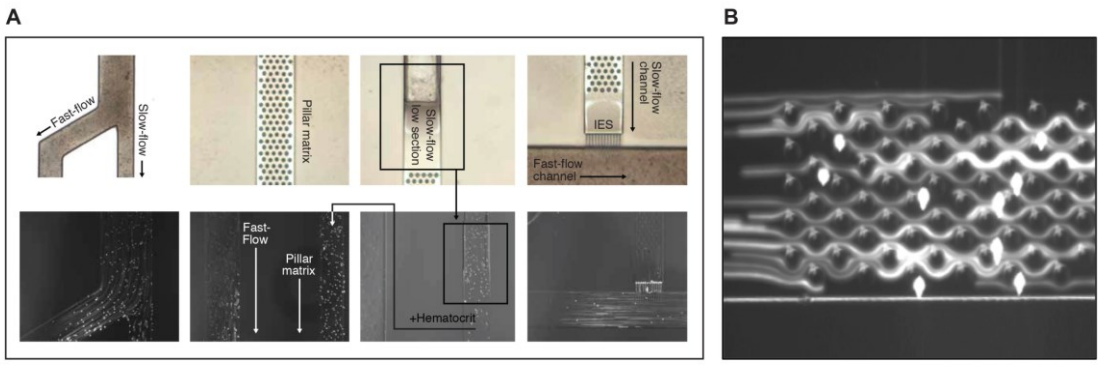

Figure S4. Microfluidic device validation. The hydrodynamic behavior of the device was tested and verified with microbeads of different diameters. These initial assays focused on the critical sections to confirm that flow motion and division in the device was similar to that of the actual spleen on a proportional scale. Also, it was pivotal to examine the demeanor of the pillar matrix section to confirm that it acted as a particle retention mechanism, not as a deterministic lateral displacement step, reducing the particle speed while increasing the cell density. **(A)** Testing the microfluidic device critical sections with different fluorescent microbeads. **(B)** Pillar matrix constriction zone evaluation.

Supplementary Movie S1. Blood flow division inside the microfluidic device.

Movie showing the blood flow distribution according to what has been observed in the human spleen. Circa 90% of it goes through closed-fast microcirculation (the fast-flow channel in the oblique direction) whereas the remaining 10% goes through open-slow microcirculation (the slow-flow channel in the horizontal direction).

Supplementary Movies S2 & S3. Passage of blood through the microconstrictions of the microfluidic device mimicking the interendothelial slits.

Experiments were performed with red blood cells from BALB/c mice infected with the reticulocyte-prone nonlethal *P. yoelii* 17X constitutively expressing GFP to facilitate image acquisition. Squeezing of *P. yoelii*-infected reticulocytes can be easily detected during its passage through the microconstrictions in these movies. Blood was introduced at 5 μL/min. Movie S2 shows the passage in real time (27.9 fps) whereas movie S3 shows the passage 5.75-times slower (5fps). Both movies were taken with a laser scanning confocal microscope (TCS-SP5; Leica Microsystems) at a magnification of 25.0 x (water objective).